Atomistic modelling of water transport and adsorption mechanisms in silicoaluminophosphate for thermal energy storage

Atomistic modelling of water transport and adsorption mechanisms in silicoaluminophosphate for thermal energy storage

Matteo Fasano[1], *Gabriele Falciani*[1], *Vincenza Brancato*[2], *Valeria Palomba*[2], *Pietro Asinari*[1], *Eliodoro Chiavazzo*[1,*], *Andrea Frazzica*[2,*]

[1] Department of Energy, Politecnico di Torino, Corso Duca degli Abruzzi 24, 10129 Torino, Italy.

[2] CNR - Istituto di Tecnologie Avanzate per l'Energia "Nicola Giordano", Via Salita S. Lucia sopra Contesse 5, 98126 Messina, Italy.

* Corresponding authors: Eliodoro Chiavazzo, Ph.D.: eliodoro.chiavazzo@polito.it; Andrea Frazzica, Ph.D.: andrea.frazzica@itae.cnr.it

ABSTRACT

SAPO-34 – a silicoaluminophosphate microporous material – has recently attracted a great attention in the field of sorption thermal storage, since it is characterized by good water adsorption behavior (*i.e.* type V adsorption isotherms) and low regeneration temperature (*i.e.* 80°C, for instance available by standard solar thermal energy collectors). However, the nanoscale mechanisms of water transport and adsorption in the microporous framework of SAPO-34 cannot be fully unveiled by experiments alone. In this work, water adsorption onto SAPO-34 is for the first time studied by means of an atomistic model built upon experimental evidence. First, Monte Carlo simulations are employed to set up a convenient atomistic model of water/SAPO-34 non-bonded interactions, and numerical adsorption isotherms are validated against experimental measures. Second, the validated model is used to study the water diffusion through SAPO-34 by Molecular Dynamics simulations, and to visualize preferential adsorption sites with atomistic detail. Such atomistic model validated against experiments may ease the investigation and *in silico* discovery of silicoaluminophosphates for thermal storage applications with tailored adsorption characteristics.

KEYWORDS

Thermal energy storage, Molecular dynamics, Monte Carlo, SAPO-34, Water, Adsorption

1. INTRODUCTION

Renewable Heating and Cooling (RHC) sector is considered as the "sleeping giant" among the alternative energy technologies, since – according to several outlooks – heating and cooling will represent up to 45% of worldwide energy consumption in the next decades [1]. Among RHC technologies, an attractive one is represented by solar thermal, thanks to its technological maturity and field of applicability that ranges from domestic to industrial sector [2]. To enlarge the exploitability of these sources, a crucial component is represented by Thermal Energy Storage (TES), since it is needed to cover the mismatch – either on daily or seasonal basis – between energy supply and demand [3-5]. The basic principle of TES consists in transferring the heat, when available, to a storage media and releasing it, when necessary, to compensate for the energy source intermittency [6].

Among all technologies currently under investigation for TES, sorption systems are considered promising for both short- and long-term TES, since they couple a high energy density with a virtually loss-free storage method [7]. In fact, the reversible physisorption reaction between a fluid sorbate and a solid adsorbent allows both storing energy without heat losses over time and achieving large energy storage density [8, 9]. While water represents a common sorbate, a broad variety of solid adsorbents are available [10, 11]. Features of adsorbents (adsorption isotherm types, isosteric heat, stability, etc.) are critical for designing optimal adsorption cycles and should be carefully analyzed, especially in view of the temperature at which the thermal source is available [12]. In this respect, several types of zeolites (and zeolite-based composites) have attracted attention, mostly for their good stability and high isosteric heat [13-16].

AlPOs (aluminophosphates) and SAPOs (silicoaluminophosphates) have been extensively investigated for TES applications in the last years [17, 18]. The AlPO primary building units are formed by Al-O-P linkages instead of the typical Si-O-Al or Si-O-Si bridges of other zeolites. The crystalline structure of these materials is similar to natural and synthetic zeolites, for this reason they are often regarded as *zeotypes* [19]. SAPOs maintain the same overall structure of AlPOs, although local structural changes are found as a consequence of the introduction of silicon atoms [20]. In general, AlPOs and SAPOs share with zeolites some important properties, such as nanoscale pore dimensions and large pore surface-to-volume ratios. However, adsorption isotherms of those materials are unique, as they may show a convenient S-shaped adsorption isotherm (*i.e.* type V): this feature makes AlPOs and SAPOs interesting for heat transformation applications. To this purpose, SAPO-34 is regarded as one of the most attractive choices among AlPOs and SAPOs currently available [21]. The thermal charging process of SAPO-34 can indeed take place at lower temperatures than traditional zeolites due to its peculiar type V isotherm, and it is therefore possible to use low temperature heat (e.g. from solar thermal collectors or industrial processes) to complete the water desorption phase [19]. This is due to the fact that SAPO-34 is less hydrophilic than other traditional zeolites (e.g. 13X), thus allowing more efficient adsorption/desorption cycles. For these reasons, SAPO-34 is already employed in adsorption chillers and heat pumps that use low grade heat as energy source [22-25].

The fundamental mechanisms underlying the adsorption properties of SAPO-34 can be investigated with the support of atomistic simulations. Ghysels *et al.* optimized a model for molecular dynamics simulation of methanol to olefins process, where SAPO-34 was used as a catalyst [26]. In particular, the authors investigated the diffusion of ethene depending on temperature, composition, acidity, and topology of the adsorbent material. A wide range of

materials was considered: AlPOs, SAPOs, and isostructural aluminosilicates with different topologies (AEI, CHA, AEX). Fisher, instead, studied the interactions between SAPO-34 and water at a smaller scale, by using dispersion-corrected density-functional theory [27]. Different topologies of AlPOs and SAPOs (AEI, AFX, CHA, ERI, GIS, RHO) were compared and studied as well: in particular, the arrangement of the framework protons of SAPOs and their affinity with water molecules were investigated.

Despite the above efforts, it is fair to say that the nanoscale mechanisms of water transport and adsorption in the microporous framework of SAPO-34 have not been fully unveiled by numerical and experimental studies so far. In particular, to our knowledge, an accurate force field parametrization for classical atomistic modelling of water in SAPO-34 is still missing. As such, here we propose a comprehensive effort where Monte Carlo (MC) simulations, classical Molecular Dynamics (MD) and experimental validation are synergistically used to get a better understanding of the above phenomena, thus moving towards an *in silico* estimate of adsorption equilibrium isotherms as well as water transport and distribution through SAPO-34 [28, 29]. Those quantities are of primary importance to calculate the achievable thermodynamic performance (e.g. energy storage density, thermal charge/discharge duration) of adsorption working pairs and, in perspective, to develop novel zeolite-like adsorbents (zeotypes) with promising thermal storage capability by means of a computational-driven approach [30].

2. MATERIAL CHARACTERIZATION

Setting up a robust atomistic model of water/SAPO-34 system required a preliminary characterization activity. The adsorbent material considered for the experimental tests is a commercial SAPO-34 produced by Mitsubishi Plastic Inc., known as AQSOA Z02 [31].

2.1. Structural properties

SAPO-34 has a CHA (chabazite) topology, where the basic unit is a tetrahedral structure composed by oxygens and T-atoms (silicon, phosphorus or aluminum). The trigonal CHA structure includes two types of cages: large 20-hedral CHA cages with 36 T atoms (0.94 nm in diameter), and smaller 8-hedral double 6-ring units (0.38 nm in diameter) [32, 33].

First, X-ray diffraction (XRD) analysis was carried out on the SAPO-34 sample to highlight possible discrepancies from the pure chabazite structure. The experiments were performed using a Philips X'PERT diffractometer, with a monochromatic Cu K radiation (λ = 1.54056 Å) at 30 kV and 20 mA. The considered 2θ interval ranges between 5° and 50°. A reasonably good matching between experimental and theoretical chabazite structure is visible in **Figure 1a**. Nevertheless, looking at the diffraction pattern, we can also observe that a certain amount of amorphous material is present in the considered SAPO-34 sample, as testified by the background visible from the X-ray pattern. The presence of the not crystalline fraction might be due to an incomplete crystallization of the material during its synthesis. Furthermore, a slight deviation of the main peaks from the theoretical diffraction pattern is observed, which could depend on the calcination process required to remove the template from the adsorbent material. Additionally, it is important to notice that the composition of AQSOA Z02 may be slightly different from pure SAPO-34, since the former was optimized for adsorption chillers application through an undisclosed formulation and synthesis process [34].

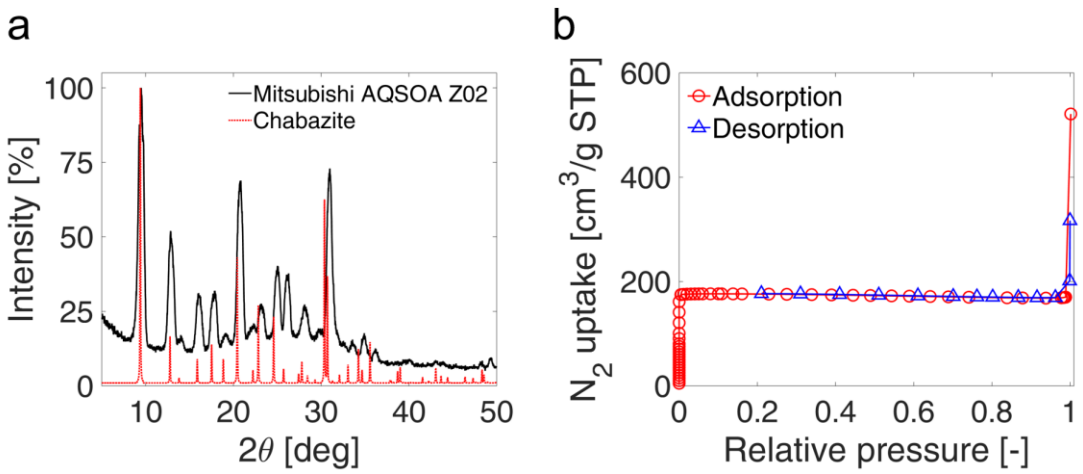

Figure 1. (a) XRD analysis of the considered SAPO-34 sample (Mitsubishi AQSOA Z02), as compared with the pure, theoretical structure of chabazite. **(b)** Isotherm of nitrogen physisorption onto SAPO-34 sample, at 77 K.

Second, Micromeritics ASAP 2020 was employed to measure the texture properties of SAPO-34 sample by nitrogen physisorption. As expected, the nitrogen physisorption is described by a type I isotherm (see **Figure 1b**). No adsorption/desorption hysteresis can be noticed due to the pure microporous structure of material. The specific surface area of SAPO-34 sample, calculated by the Langmuir model, is 765.6 m^2/g: this value is consistent with data from Mitsubishi, which lie in the 650–770 m^2/g range [35]. Moreover, the total pore volume is measured as 0.262 cm^3/g; whereas, the size of the median pore calculated with the Horvath-Kawazoe method is about 0.509 nm, which is consistent with the typical CHA structure composed by large (0.94 nm in diameter) and small (0.38 nm in diameter) cages.

2.2. Adsorption isotherms

The water adsorption isotherms of SAPO-34 were experimentally measured at various temperatures by a Dynamic gravimetric Vapour Sorption analyser (DVS vacuum, see **Figure 2**), with partial pressures spanning from 0 to 0.9. The device measures gravimetrically the water

uptake and loss of SAPO-34, using a SMS ultra-balance with mass sensitivity of 0.1 μg. The water vapour pressure surrounding the sample was regulated by a mass flow controller. The temperature (T) was maintained constant (±0.1 K) by enclosing the manifold in a temperature-controlled incubator. The SAPO-34 sample (ca. 10 mg) was loaded into the specimen pan and then placed into the instrument. Before being exposed to any vapour flow, the sample was degassed in situ at 453 K under vacuum (≈133 Pa) for 8–12 h, to desorb any prior physisorbed moisture. Afterwards, the sample was exposed to the desired pressure, and the vapour uptake was monitored under dynamic water vapour flow. A series of equilibrium points were acquired by measuring the sample weight variation in response to a stepwise partial pressure change.

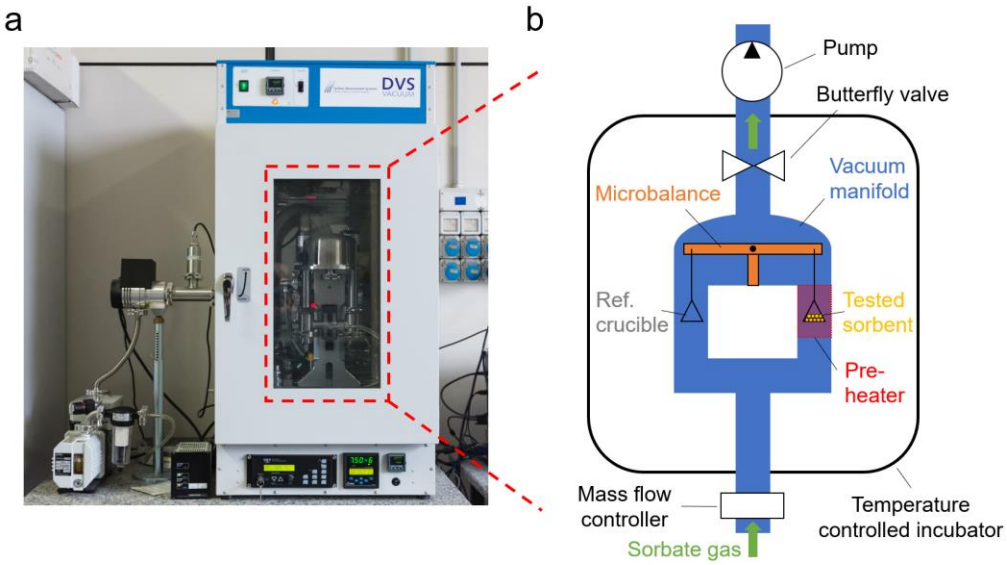

Figure 2. Dynamic gravimetric vapor sorption analyzer: **(a)** overall view of the apparatus installed at the CNR-ITAE lab; **(b)** schematic of the working principle for the thermogravimetric measure. The pre-heater is employed to precisely control the sample temperature and to perform desorption experiments.

Figure 3 reports the adsorption isotherms obtained at T = 303 K, 313 K, 323 K, and 333 K. As expected, all the measured isotherms present an S-shaped evolution in the range 0–0.25 p/p_0 (p_0 is the saturation pressure), therefore belonging to type V isotherms. Furthermore, a certain

degree of hysteresis between adsorption and desorption isotherms can be found per each test. Notice that the error bars in the experimental adsorption isotherms are indistinguishable from the reported mean values, since the accuracy of the dynamic gravimetric vapour sorption analyser is in the order of few micrograms. A comparison among the experimental equilibrium data measured in this work and literature data is reported in **Figure 4**. The measured adsorption isotherms were almost at the same temperature (*i.e.* maximum difference 5 K), showing, in general, a good agreement. The only deviation is shown by the measurements reported by Kayal *et al.* [31], whose isotherms underestimate the adsorption capacity of the material. This can be justified by the different experimental methodology employed, *i.e.* volumetric method instead of gravimetric one. Nevertheless, they confirm the same isotherm shape as for the other tests.

The isosteric heat of adsorption (q_{st}) can be then calculated from adsorption isotherms on the basis of the van't Hoff equation derived from the Clausius-Clapeyron relation [36], namely

$$q_{st} = -R \left. \frac{\partial(\ln p)}{\partial\left(-\frac{1}{T}\right)} \right|_{w=const}, \quad (1)$$

being R the ideal gas constant and w the water uptake level. Considering the adsorption isotherms reported in **Figure 3**, **Equation 1** provides an average isosteric heat of adsorption of water onto SAPO-34 equal to 61.8 kJ/mol in the range 0–0.4 p/p_0, in good agreement with previous values available in the literature [37, 38].

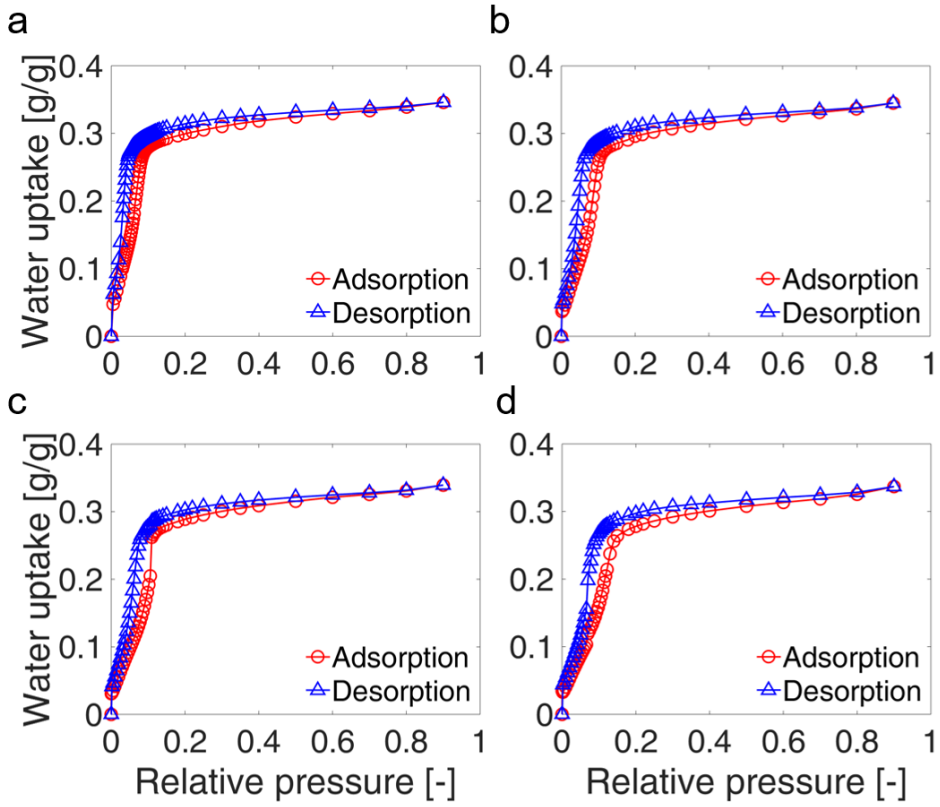

Figure 3. Water adsorption isotherms experimentally measured for the SAPO-34 (AQSOA Z02) sample at different temperatures: **(a)** 303 K; **(b)** 313 K; **(c)** 323 K; **(d)** 333 K. Both adsorption and desorption curves are represented; error bars are indistinguishable from mean values since they are in the order of few micrograms per gram.

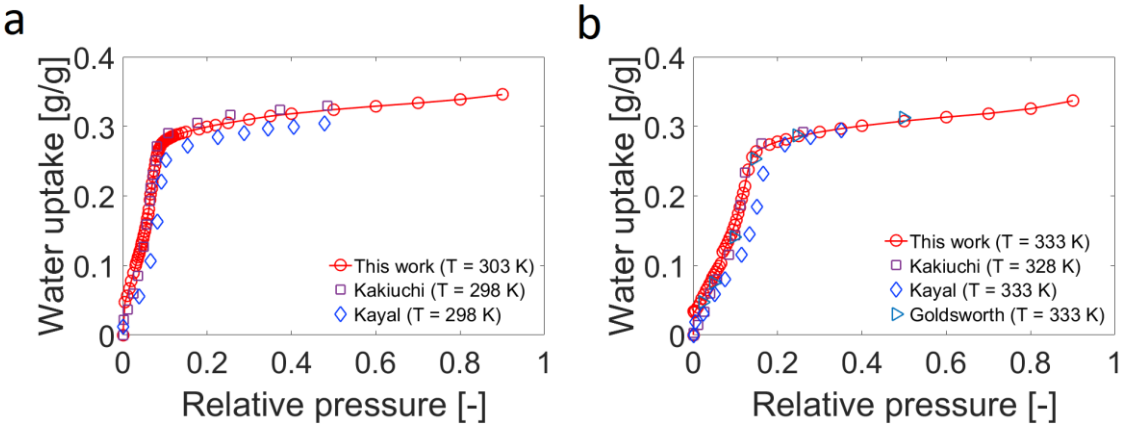

Figure 4. Comparison between measured water adsorption isotherms of SAPO-34 (AQSOA Z02) and data from Kayal *et al.* [31], Kakiuchi *et al.* [39], and Goldsworth [40], at about **(a)** 303 K and **(b)** 333 K.

3. MATERIAL MODELLING

The mechanisms of water adsorption and transport in SAPO-34 zeotype are here investigated at the molecular scale by classical atomistic simulations. Both Monte Carlo and molecular dynamics simulations were employed to compute adsorption isotherms and transport properties, respectively [28]. In this section, the detailed configurations and interaction potentials adopted in the simulations are first presented; the simulated adsorption isotherms for the water/SAPO-34 adsorption couple are then compared with experimental results and transport properties of water through SAPO-34 reported.

3.1. Atomistic configuration

The considered unit cell of SAPO-34 crystal has $3[Al_6P_5SiO_2\ 3(OH)]$ atomic composition, with a total of 111 atoms [26]. Starting from this unit cell ($a = b$ =13.95 Å, c =14.95 Å; $\alpha = \beta$ =90°, γ =120°), the geometry was transformed into a orthorhombic crystalline structure (a =23.80 Å, b =27.50 Å, c =29.50 Å; $\alpha = \beta = \gamma$ =90°) by VESTA [41] and Crystal Maker software, as depicted in **Figure 5a**. During simulations, this configuration was considered periodic along x, y, and z Cartesian axes.

In this study, we have mostly followed the work of Ghysels *et al.* for modeling the interaction potential parameters [26]. However, owing to the different sorbate molecule considered here, we also suggest a few adjustments to more accurately describe water adsorption within SAPO-34. More specifically, molecular interactions were modelled by both bonded and non-bonded potentials. Bonded interactions are due to intramolecular chemical bonds. Bond stretching (2-body) interactions of OH terminals of SAPO-34 were modelled by Morse potential; whereas, the other bond stretching interactions by harmonic potentials. Angle (3-body)

interactions were all mimicked by harmonic potentials. Non-bonded interactions arise from both van der Waals and electrostatic forces, which were modelled here by 12-6 Lennard-Jones and Coulomb potentials, respectively. Non-bonded interactions between framework atoms included not only T-O (T=Si, Al, P) and O-O terms, but also T-T interactions. TIP4P/2005 was employed as water model [42], while Lorentz-Berthelot rules were considered to compute cross Lennard-Jones terms. The detailed list of parameters of bonded and Lennard-Jones potentials for SAPO-34 can be taken from the previous work by Ghysels *et al*. [26]; whereas, the partial charge values of the adsorbent structure have been optimized in the followings to best model the water uptake process observed in the experiments.

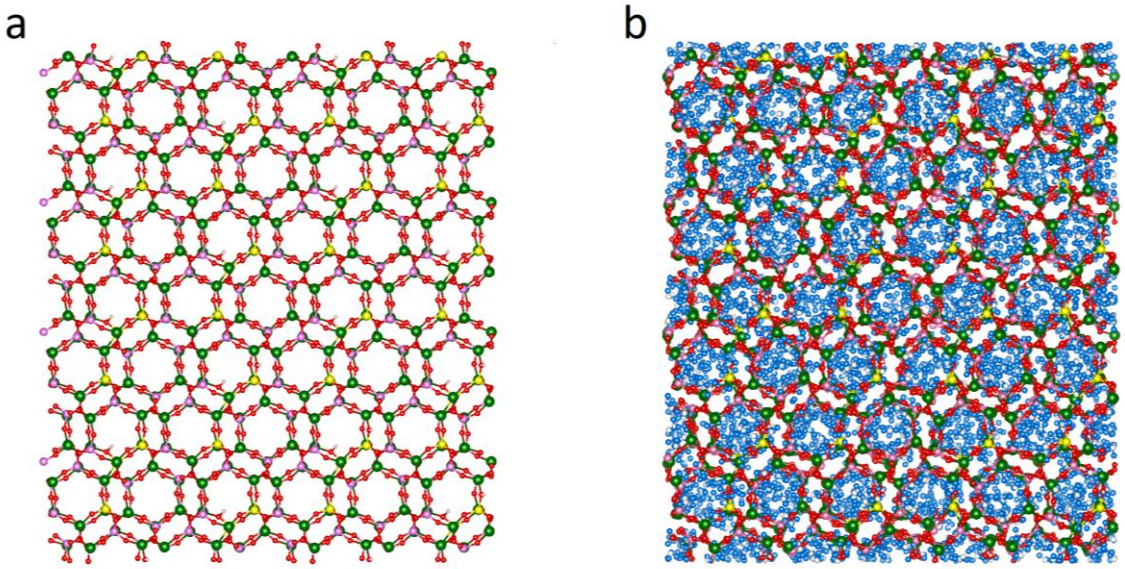

Figure 5. (a) Dry configuration of SAPO-34 considered in the simulations. **(b)** Fully hydrated (water uptake equal to 0.32 g/g) configuration of SAPO-34, where water molecules are depicted in light blue.

3.2. Water adsorption by Monte Carlo

Grand Canonical Monte Carlo simulations (GCMC) were performed by MUSIC software [43] to measure the equilibrium amount of adsorbed water molecules at fixed chemical potential (μ),

volume (V), and temperature (T). During GCMC runs, the SAPO-34 framework is considered as fixed and, therefore, only non-bonded interactions are taken into account.

In detail, the Monte Carlo simulation protocol starts with the preliminary creation of two lookup tables, namely *Emap* and *Pmap*. The GCMC simulation then uses these lookup tables to interpolate interaction potentials between the grid points, instead of calculating them at each iteration. On the one hand, *Emap* describes the electrostatic potential experienced by one generic sorbate atom with unit charge in all the possible positions in the microporous sorbent, considering an approximate grid spacing of 0.6 Å. On the other hand, *Pmap* is generated evaluating the Lennard Jones potential felt by each atom of the considered sorbate (water in this case) in all the possible positions in the microporous sorbent (SAPO-34 in this case), with an approximate grid spacing of 0.5 Å.

After these preliminary steps, three computational boxes were created from the initial unit cell of SAPO-34 (111 atoms, referred to as box 0). Once the orthorhombic geometry was generated (222 atoms, referred to as box 1), the box size has been scaled: as a first step, a duplication along one axis was performed (444 atoms, referred to as box 2); then, by doubling the size along a second axis, we obtained box 3 (888 atoms); finally, the box size was doubled again along the third axis, thus obtaining box 4 (1776 atoms).

A convergence analysis of GCMC simulations was performed using the orthorhombic boxes (box 2, 3 and 4) at $p = 1.5$ kPa ($p/p_0 = 0.2$) and $T = 313$ K, and results are reported in **Figure 6**. As a reference, the horizontal dashed line represents the experimental water uptake at p/p_0 = 0.2 and T = 313 K. It is important to note that the computational time increases significantly with the size of simulation box; whereas, the maximum cut-off radius of non-bonded interactions that can be employed in the GCMC runs is equal to half of the shortest box

side. Simulations with box 2 were the fastest (less than 1 day per run, in average), considering a fixed number of iterations; however, due to the limited box size, the maximum cut-off radius of non-bonded interactions was 7.3 Å. Such short cut-off radius may cause potential truncation and thus detrimental effects on simulation accuracy. Considering box 4, instead, the computational time necessary to simulate the minimum number of iterations required to achieve convergence of results was prohibitive for our facilities (more than 1 month per run). Finally, simulations performed with box 3 showed a good convergence at 200 million iterations consistently with other works in literature [44], with a reasonable computational time (less than 1 week per run) and cut-off radius (11.0 Å). Therefore, box 3 is adopted in the following analyses as the best compromise between simulation accuracy and computational time.

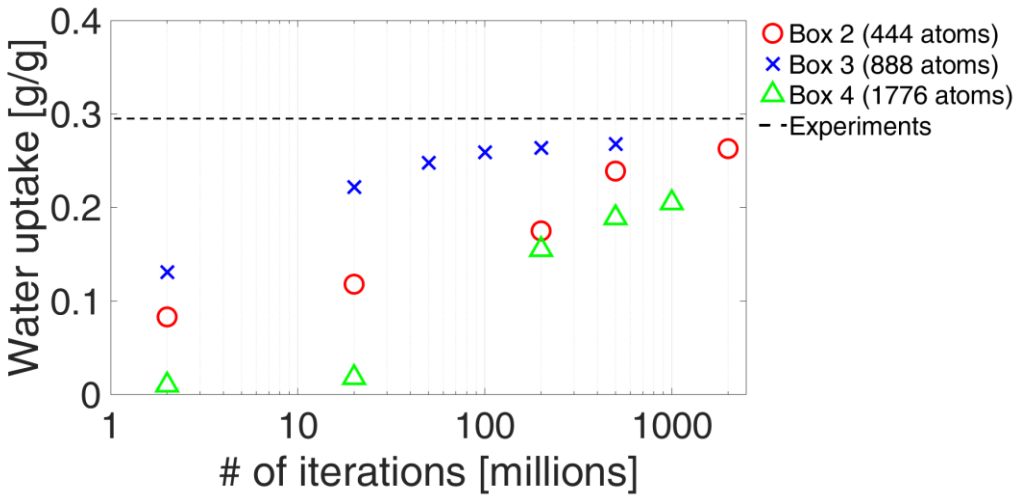

Figure 6. Convergence analysis for the different boxes simulated by Monte Carlo method, at p = 1.5 kPa and T = 313 K. Simulations are done with the optimized force field (FF reference + 6% q_O, see **Table 1**).

The complete water adsorption isotherm was first calculated using the original force field parametrization by Ghysels *et al*. [26]. To improve the statistic relevance of numerical results, 4 repetitions (200 million iterations each) with different seed numbers were conducted per each considered relative pressure, and the obtained water uptakes averaged. The adsorption curve was

calculated up to a partial pressure of 0.2 and at T = 313 K, and it is depicted in **Figure 7a** (red stars). Results show that the typical S-shaped isotherm of SAPO-34 is recovered by the MC model as well; however, experiments significantly deviate from numerical predictions (Mean Absolute Percentage Error - MAPE approximately equal to 38% considering $p/p_0 > 0.01$). Motivated by the latter observation, we have investigated possible changes to the initial force field parametrization that might result in a better fitting of the experimental data.

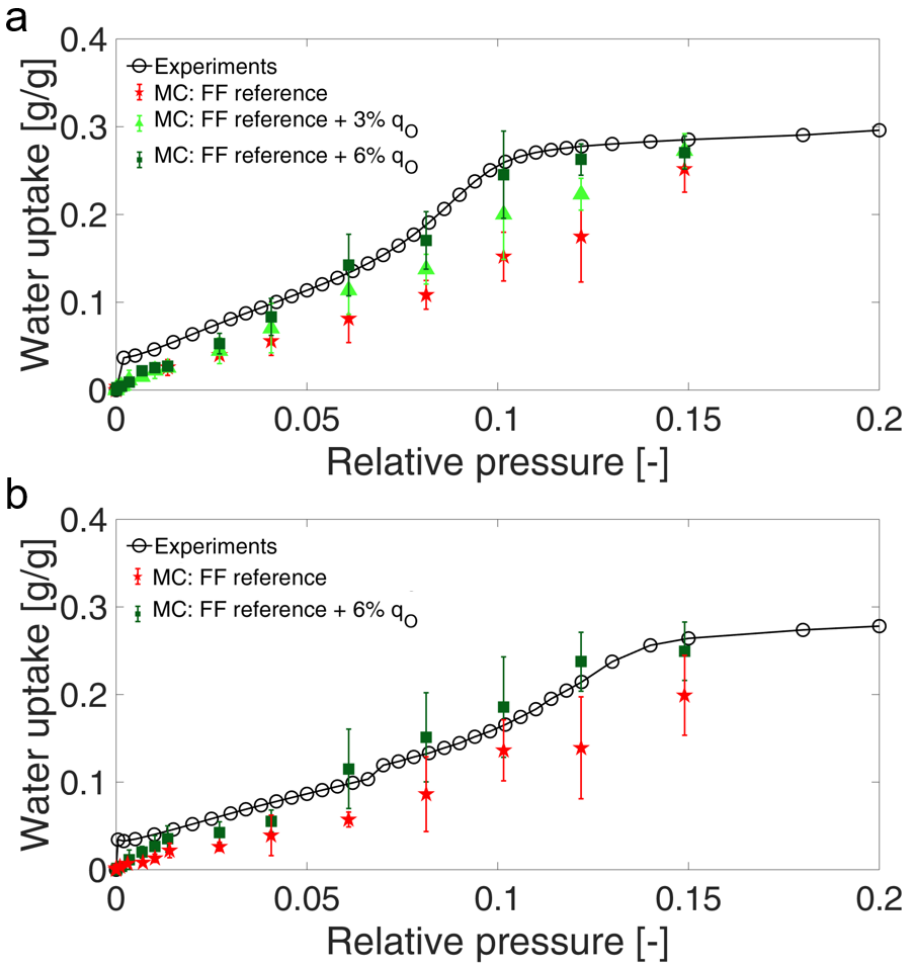

Figure 7. Comparison between the experimental adsorption isotherm and the corresponding Monte Carlo results with different force field parametrization (see **Table 1**). Red stars represent simulation results using the reference force field by Ghysels *et al.* [26]. Different adsorption temperatures are considered: **(a)** 313 K; **(b)** 333 K. Error bars of simulations are standard deviations of 4 repetitions conducted with different seed numbers. Note that the relative pressure is intended as p/p_0, being p_0 the saturation pressure; whereas, the uptake is reported as grams of adsorbed water per grams of adsorbent.

Therefore, non-bonded electrostatic parameters were varied to assess their influence on adsorption curve [28]. Specifically, partial charges of oxygen atoms of SAPO-34, both O1 and O2, were increased by 3% in a first simulation (left-hand side of **Table 1**), and by 6% in a second one (right-hand side of **Table 1**) respect to the reference force field by Ghysels *et al*. [26]. Moreover, the partial charges of the other framework atoms were modified as well, so that their ratio was maintained constant and the overall charge neutrality of the crystal preserved. The computed adsorption isotherms are reported in **Figure 7a**. As expected, SAPO-34 hydrophilicity is enhanced by larger partial charges, therefore increasing the water uptake at given pressure. Among all options explored in this study, the force field with partial charges of oxygen atoms increased by 6% provides the best fitting with the adsorption experimental data (MAPE ≅10% considering p/p_0> 0.01). Notably, this is almost a four times improvement respect to the original force field. To verify the transferability of the modified force field parametrization, we have also computed the adsorption isotherm at 333 K: results in **Figure 7b** confirm that the new force field can be used with satisfactory accuracy also for different adsorption temperatures (MAPE ≅15% considering p/p_0> 0.01), with discrepancies mostly noticed at relative pressures below 0.1.

FF reference + 3%		**FF reference + 6%**	
Atom	q [e]	Atom	q [e]
Si	2.1630	Si	2.2260
Al	1.6223	Al	1.6695
P	2.7038	P	2.7825
O1	-0.7468	O1	-0.7685
O2	-1.0815	O2	-1.1130
H1	0.2060	H1	0.2120

Table 1. Partial charges changes with respect to the reference force field parametrization suggested by Ghysels *et al*. [26]. Left: non-bonded electrostatic parameters of SAPO-34 with an increase of 3% of O1 and O2 partial charges respect to the reference force field. Right: non-bonded electrostatic parameters of SAPO-34 with an increase of 6% of O1 and O2 partial charges respect to the reference force field. The charges of other atoms of SAPO-34 are changed to keep an overall neutral charge in the zeotype structure.

3.3. Water transport and distribution by Molecular Dynamics

The atomistic model of water/SAPO-34 validated by MC simulations against experimental adsorption isotherms was then employed to study water transport within the zeotype pores. To this purpose, the self-diffusivity of water molecules within SAPO-34 was computed by molecular dynamics simulations through GROMACS software [45]. The influence of hydration level on the water self-diffusivity was studied by simulating SAPO-34 with an increasing amount of adsorbed water molecules, spanning from 10% to 100% of the maximum water uptake achieved at saturation pressure.

The optimized force field found by previous Monte Carlo simulations was chosen; whereas, a larger simulation box of SAPO-34 (59.0x47.6x55.0 $Å^3$, periodic boundary conditions) was conveniently employed to reduce fluctuations. Both electrostatics and Van der Waals cut off radii have been set to 1.3 nm. The hydrated configuration (**Figure 5b**) was first energy minimized (steepest descent algorithm) and then thermalized in the canonical ensemble (velocity rescaling thermostat at $T = 313$ K [46]; 0.3 ns trajectories). The isotropic self-diffusion coefficient of adsorbed water molecules was finally computed from the mean square displacement via the Einstein's relation [47], considering trajectories simulated in the canonical ensemble (Nosé-Hoover thermostat at $T = 313$ K [48]; 2 ns trajectories).

As shown in **Figure 8**, increasing water uptake causes a reduction in the self-diffusion coefficient of adsorbed water, mainly due to the enhanced sorbate-sorbate interactions at higher hydrations [49]. Furthermore, since the bulk self-diffusion coefficient of TIP4P water is computed as (2.66 +/- 0.01) $\times 10^{-9}$ m^2/s (T =313 K and p =1 bar, simulation in the isothermal-isobaric ensemble for 10 ns) and self-diffusivities in **Figure 8** are one order of magnitude lower, the water molecules adsorbed onto the hydrophilic surface of SAPO-34 pores undergo strong

nanoconfined conditions, coherently with previous observations in the literature [47, 49-51]. The analysis of MD trajectories also allows to visualize the mean distribution and local density of water molecules within SAPO-34, to highlight their preferential adsorption sites. **Figure 9** presents the water density maps within SAPO-34 at fully hydrated conditions (water uptake=0.32 g/g), where water molecules aggregates can be observed preferentially in the bigger cages of zeotype framework.

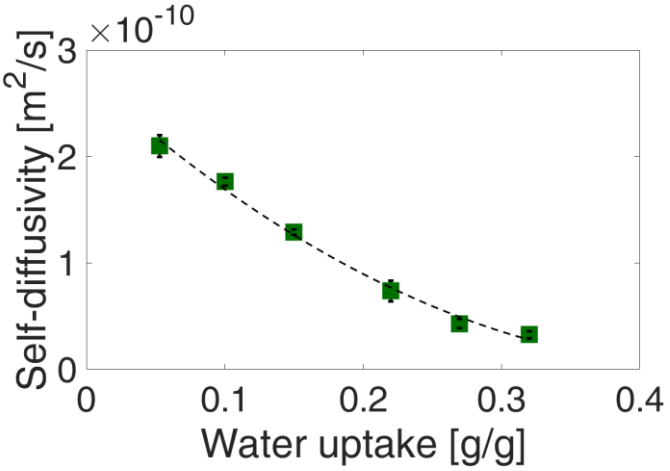

Figure 8. Self-diffusion coefficient of water molecules within the simulated SAPO-34 framework, at increasing hydration levels (T = 313 K). Simulations are carried out by molecular dynamics with the optimized force field of SAPO-34 (FF reference +6% q_O, see **Table 1**). As a reference, the bulk self-diffusivity of TIP4P water at the same temperature is computed as (2.66 +/- 0.01) $\times 10^{-9}$ m^2/s. Note that the water uptake is reported as grams of adsorbed water per grams of adsorbent. Error bars are reported as ± one standard deviation. The black dashed line is a guide for eyes.

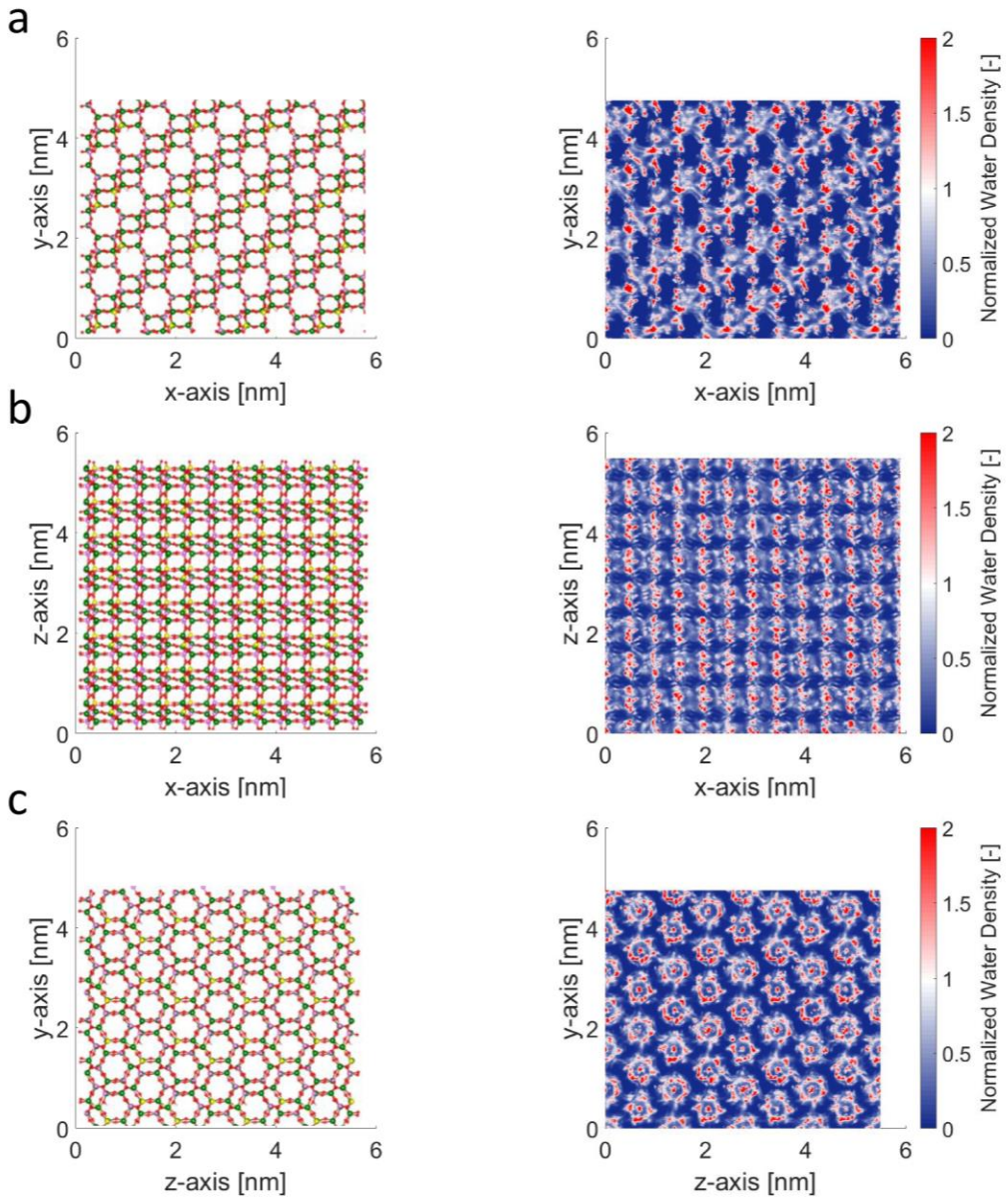

Figure 9. Water density within SAPO-34, as obtained from molecular dynamics simulations at fully hydrated conditions (water uptake=0.32 g/g). Left column: view of simulated SAPO-34 framework (water molecules are not shown for clarity). Right column: density maps of water adsorbed onto SAPO-34 framework. The local density of water is normalized by the simulated density of bulk water at 313 K and 1 bar (991.3 kg/m^3). **(a)** x-y view; **(b)** x-z view; **(c)** z-y view.

4. CONCLUSIONS

Microporous materials characterized by S-shaped water adsorption isotherms (for example, SAPO-34) allow getting high water exchange in an extremely narrow temperature range, thus

increasing the achievable thermal storage density at the typical working conditions of systems driven by renewable energy sources. In this work, water adsorption onto SAPO-34 is for the first time studied by means of an atomistic model built upon experimental evidence. First, the water adsorption properties of a commercial SAPO-34 (AQSOA Z02) were experimentally investigated by means of a thermo-gravimetric analysis under wide temperature and relative pressure range. Subsequently, water/SAPO-34 adsorption working pair was investigated by atomistic simulations. Both Monte Carlo and molecular dynamics models were employed to simulate adsorption isotherms, water self-diffusivity and distribution within the zeotype framework.

A previously suggested force field parametrization was here modified to best fit our experimental results. By such a modification, an overall good agreement was achieved in terms of adsorption isotherms at different temperatures, thanks to a four times accuracy improvement respect to the original force field. On the other hand, the suggested refined force field parametrization can be certainly considered as a first critical step towards more accurate atomistic predictions of equilibrium adsorption properties of the water/SAPO-34 pair, since discrepancies are still noticeable at near-zero water coverage. However, to some extent, the currently unknown precise material formulation of commercially available SAPO-34 (AQSOA Z02) is generating an unavoidable uncertainty in the study (as also demonstrated by the reported XRD analysis) and it can be resolved only upon full disclosure of the detailed atomistic composition in the future.

In perspective, chemically precise and experimentally validated atomistic models of water adsorption onto SAPO and AlPO materials may constitute a robust physical basis for the *in silico* discovery of novel zeolite-like adsorbents for sorption heat storage applications.

REFERENCES

[1] D. Ürge-Vorsatz, L.F. Cabeza, S. Serrano, C. Barreneche, K. Petrichenko, Heating and cooling energy trends and drivers in buildings, Renewable and Sustainable Energy Reviews, 41 (2015) 85-98.

[2] S.A. Kalogirou, Solar thermal collectors and applications, Progress in Energy and Combustion Science, 30 (2004) 231-295.

[3] A. Frazzica, A. Freni, Adsorbent working pairs for solar thermal energy storage in buildings, Renewable Energy, 110 (2017) 87-94.

[4] A. Andreozzi, B. Buonomo, D. Ercole, O. Manca, Solar Energy Latent Thermal Storage by Phase Change Materials (PCMs) in a Honeycomb System, Thermal Science and Engineering Progress, 6 (2018) 410-420.

[5] A. Andreozzi, B. Buonomo, D. Ercole, O. Manca, Phase change materials (PCMs) in a honeycomb system for solar energy applications, International Journal of Heat and Technology, 35 (2017) S472-S477.

[6] A. Arteconi, N.J. Hewitt, F. Polonara, State of the art of thermal storage for demand-side management, Applied energy, 93 (2012) 371-389.

[7] L. Scapino, H.A. Zondag, J. Van Bael, J. Diriken, C.C. Rindt, Sorption heat storage for long-term low-temperature applications: A review on the advancements at material and prototype scale, Applied energy, 190 (2017) 920-948.

[8] A. Hauer, Sorption theory for thermal energy storage, in: Thermal energy storage for sustainable energy consumption, Springer, 2007, pp. 393-408.

[9] B. Dawoud, E.H. Amer, D.M. Gross, Experimental investigation of an adsorptive thermal energy storage, International Journal of Energy Research, 31 (2007) 135-147.

[10] G. Santori, C. Di Santis, Optimal fluids for adsorptive cooling and heating, Sustainable materials and technologies, 12 (2017) 52-61.

[11] R. Critoph, Y. Zhong, Review of trends in solid sorption refrigeration and heat pumping technology, Proceedings of the Institution of Mechanical Engineers, Part E: Journal of Process Mechanical Engineering, 219 (2005) 285-300.

[12] Z. Lu, Z. Xia, D. La, Experimental study with operational solar-sorption cooling, International Journal of Energy Research, 37 (2013) 673-682.

[13] R. van Alebeek, L. Scapino, M. Beving, M. Gaeini, C. Rindt, H. Zondag, Investigation of a household-scale open sorption energy storage system based on the Zeolite 13X/water reacting pair, Applied Thermal Engineering, 139 (2018) 325-333.

[14] A. Ristić, F. Fischer, A. Hauer, N.Z. Logar, Improved performance of binder-free zeolite Y for low-temperature sorption heat storage, Journal of Materials Chemistry A, 6 (2018) 11521-11530.

[15] D. Dicaire, F.H. Tezel, Use of adsorbents for thermal energy storage of solar or excess heat: improvement of energy density, International Journal of Energy Research, 37 (2013) 1059-1068.

[16] L. Shere, S. Trivedi, S. Roberts, A. Sciacovelli, Y. Ding, Synthesis and Characterization of Thermochemical Storage Material Combining Porous Zeolite and Inorganic Salts, Heat Transfer Engineering, (2018) 1-6.

[17] L.F. Cabeza, A. Solé, C. Barreneche, Review on sorption materials and technologies for heat pumps and thermal energy storage, Renewable Energy, 110 (2017) 3-39.

[18] V. Brancato, A. Frazzica, Characterisation and comparative analysis of zeotype water adsorbents for heat transformation applications, Solar Energy Materials and Solar Cells, 180 (2018) 91-102.

[19] E.-P. Ng, S. Mintova, Nanoporous materials with enhanced hydrophilicity and high water sorption capacity, Microporous and mesoporous materials, 114 (2008) 1-26.

[20] G. Sastre, D.W. Lewis, C.R.A. Catlow, Modeling of silicon substitution in SAPO-5 and SAPO-34 molecular sieves, The Journal of Physical Chemistry B, 101 (1997) 5249-5262.

[21] N. Yu, R. Wang, L. Wang, Sorption thermal storage for solar energy, Progress in Energy and Combustion Science, 39 (2013) 489-514.

[22] A. Sapienza, G. Gullì, L. Calabrese, V. Palomba, A. Frazzica, V. Brancato, D. La Rosa, S. Vasta, A. Freni, L. Bonaccorsi, An innovative adsorptive chiller prototype based on 3 hybrid coated/granular adsorbers, Applied energy, 179 (2016) 929-938.

[23] J. Bauer, R. Herrmann, W. Mittelbach, W. Schwieger, Zeolite/aluminum composite adsorbents for application in adsorption refrigeration, International Journal of Energy Research, 33 (2009) 1233-1249.

[24] A. Freni, L. Bonaccorsi, L. Calabrese, A. Caprì, A. Frazzica, A. Sapienza, SAPO-34 coated adsorbent heat exchanger for adsorption chillers, Applied Thermal Engineering, 82 (2015) 1-7.

[25] U. Wittstadt, G. Füldner, E. Laurenz, A. Warlo, A. Große, R. Herrmann, L. Schnabel, W. Mittelbach, A novel adsorption module with fiber heat exchangers: Performance analysis based on driving temperature differences, Renewable Energy, 110 (2017) 154-161.

[26] A. Ghysels, S.L. Moors, K. Hemelsoet, K. De Wispelaere, M. Waroquier, G. Sastre, V. Van Speybroeck, Shape-selective diffusion of olefins in 8-ring solid acid microporous zeolites, The Journal of Physical Chemistry C, 119 (2015) 23721-23734.

[27] M. Fischer, Interaction of water with (silico) aluminophosphate zeotypes: a comparative investigation using dispersion-corrected DFT, Physical Chemistry Chemical Physics, 18 (2016) 15738-15750.

[28] M. Fasano, D. Borri, E. Chiavazzo, P. Asinari, Protocols for atomistic modeling of water uptake into zeolite crystals for thermal storage and other applications, Applied Thermal Engineering, 101 (2016) 762-769.

[29] M. Fasano, D. Borri, A. Cardellini, M. Alberghini, M. Morciano, E. Chiavazzo, P. Asinari, Multiscale simulation approach to heat and mass transfer properties of nanostructured materials for sorption heat storage, Energy Procedia, 126 (2017) 509-516.

[30] M. Tatlier, G. Munz, S.K. Henninger, Relation of water adsorption capacities of zeolites with their structural properties, Microporous and mesoporous materials, 264 (2018) 70-75.

[31] S. Kayal, S. Baichuan, B.B. Saha, Adsorption characteristics of AQSOA zeolites and water for adsorption chillers, International Journal of Heat and Mass Transfer, 92 (2016) 1120-1127.

[32] S.H. Ahn, H. Lee, S.B. Hong, Crystallization mechanism of cage-based, small-pore molecular sieves: a case study of CHA and LEV structures, Chemistry of Materials, 29 (2017) 5583-5590.

[33] Q. Sun, Z. Xie, J. Yu, The state-of-the-art synthetic strategies for SAPO-34 zeolite catalysts in methanol-to-olefin conversion, National Science Review, (2017).

[34] H. Watanabe, T. Takewaki, M. Yamazaki, H. Kakiuchi, K. Inagaki, A. Kosaka, N. Hosokawa, Zeolite, method for production thereof, adsorbent comprising said zeolite, heat utilization system, adsorption heat pump, heating and cooling storage system and humidity controlling air-conditioning apparatus in, Mitsubishi Plastics Inc, 2003.

[35] M. Chemical, Zeolite AQSOA™, in, Vol. 2018, 2018.

[36] Y.I. Aristov, Adsorptive transformation of heat: principles of construction of adsorbents database, Applied Thermal Engineering, 42 (2012) 18-24.

[37] B. Sun, A. Chakraborty, Thermodynamic formalism of water uptakes on solid porous adsorbents for adsorption cooling applications, Applied physics letters, 104 (2014) 201901.

[38] J. Jänchen, H. Stach, Shaping adsorption properties of nano-porous molecular sieves for solar thermal energy storage and heat pump applications, Solar Energy, 104 (2014) 16-18.

[39] H. Kakiuchi, S. Shimooka, M. Iwade, K. Oshima, M. Yamazaki, S. Terada, H. Watanabe, T. Takewaki, Water Vapor Adsorbent FAM-Z02 and Its Applicability to Adsorption Heat Pump, KAGAKU KOGAKU RONBUNSHU, 31 (2005) 273-277.

[40] M. Goldsworthy, Measurements of water vapour sorption isotherms for RD silica gel, AQSOA-Z01, AQSOA-Z02, AQSOA-Z05 and CECA zeolite 3A, Microporous and mesoporous materials, 196 (2014) 59-67.

[41] K. Momma, F. Izumi, VESTA 3 for three-dimensional visualization of crystal, volumetric and morphology data, Journal of Applied Crystallography, 44 (2011) 1272-1276.

[42] J.L. Abascal, C. Vega, A general purpose model for the condensed phases of water: TIP4P/2005, The Journal of chemical physics, 123 (2005) 234505.

[43] A. Gupta, S. Chempath, M.J. Sanborn, L.A. Clark, R.Q. Snurr, Object-oriented programming paradigms for molecular modeling, Molecular Simulation, 29 (2003) 29-46.

[44] C.E. Ramachandran, S. Chempath, L.J. Broadbelt, R.Q. Snurr, Water adsorption in hydrophobic nanopores: Monte Carlo simulations of water in silicalite, Microporous and mesoporous materials, 90 (2006) 293-298.

[45] S. Pronk, S. Páll, R. Schulz, P. Larsson, P. Bjelkmar, R. Apostolov, M.R. Shirts, J.C. Smith, P.M. Kasson, D. Van Der Spoel, GROMACS 4.5: a high-throughput and highly parallel open source molecular simulation toolkit, Bioinformatics, 29 (2013) 845-854.

[46] G. Bussi, D. Donadio, M. Parrinello, Canonical sampling through velocity rescaling, The Journal of chemical physics, 126 (2007) 014101.

[47] E. Chiavazzo, M. Fasano, P. Asinari, P. Decuzzi, Scaling behaviour for the water transport in nanoconfined geometries, Nature communications, 5 (2014) 3565.

[48] W.G. Hoover, Canonical dynamics: equilibrium phase-space distributions, Physical review A, 31 (1985) 1695.

[49] M. Fasano, T. Humplik, A. Bevilacqua, M. Tsapatsis, E. Chiavazzo, E.N. Wang, P. Asinari, Interplay between hydrophilicity and surface barriers on water transport in zeolite membranes, Nature communications, 7 (2016) 12762.

[50] M. Fasano, E. Chiavazzo, P. Asinari, Water transport control in carbon nanotube arrays, Nanoscale research letters, 9 (2014) 559.

[51] A. Cardellini, M. Fasano, E. Chiavazzo, P. Asinari, Interfacial water thickness at inorganic nanoconstructs and biomolecules: Size matters, Physics Letters A, 380 (2016) 1735-1740.

ACKNOWLEDGMENTS

Authors are grateful to Daniele Borri and Giacomo D'Alessandro for performing preparatory simulations and for useful discussions.

ADDITIONAL INFORMATION

The authors declare no competing financial interests.